J. Fluid Mech. (1987), *vol.* 174, *pp.* 1–22
Printed in Great Britain

On the sheared density interface of an entraining stratified fluid

By SIAVASH NARIMOUSA† AND HARINDRA J. S. FERNANDO‡
Department of Earth and Planetary Sciences, The Johns Hopkins University, Baltimore, MD 21218, USA

(Received 10 December 1984 and in revised form 4 March 1986)

This paper deals with the nature of the entrainment interface of a two-layer fluid subjected to interfacial velocity shear. The shear flow was generated by driving the mixed layer over the dense layer by a disk pump such that there is no stress at the top of the mixed layer. During the entrainment process a sharp, thin-density interfacial layer developed; its thickness δ was found to increase linearly with the mixed-layer depth h, independent of the Richardson number Ri_u. The shear layer thickness δ_s was found to be much larger than δ and the ratio δ_s/h is also found to be constant, irrespective of Ri_u. At the entrainment interface, the estimated buoyancy flux and the dissipation of turbulent kinetic-energy appear to be of the same order. This result supports an entrainment law of the form $E \sim Ri_u^{-1}$, where E is the entrainment coefficient. The interfacial layer showed sporadic large-amplitude wave oscillations whose amplitudes scaled well with the estimated size of the undulations caused by the impingement of large eddies (of size h) on the density interface. The density-interfacial layer was found to be 'topped' by a layer of partially mixed fluid which had not yet incorporated into the well-mixed region.

1. Introduction

There are numerous instances where a detailed knowledge of the effect of velocity shear on a density interface is important. For example, drift currents in the upper ocean or winds in the atmosphere play a major role in the growth of well-mixed layers against the stratification of the oceanic pycnocline or the atmospheric inversion zones. These and the associated phenomena, such as clear-air and upper-oceanic turbulence, have a direct bearing on the world's climate, the dispersion of contaminants in the ocean and atmosphere, and gas transfer across the air–sea interface (Long 1973; Fischer *et al.* 1979). According to Phillips (1977*a*), upper-ocean mixing may be responsible for bringing nutrients from the deep sea to the surface layers. In coal mines, methane gas rises and spreads horizontally as a gravity current and the extent to which it mixes with the surrounding air has an important bearing on safety (Ellison & Turner 1959). These, together with many other applications, have inspired the large number of studies on stratified shear flows. Many laboratory experiments deal with only a single mixing mechanism and try to compress the global scales of

† Present address: Department of Mechanical Engineering, University of Southern California, Los Angeles, CA 90089, USA.
‡ Present address: Department of Environmental Engineering Science, California Institute of Technology, Pasadena, CA 91125, and Department of Mechanical and Aerospace Engineering, Arizona State University, Tempe, AZ 85287, USA.

time and space to the laboratory scales. By so doing, we pay the price of removing ourselves from real geophysical situations in which the different processes that contribute to mixing interact with each other. Nevertheless, such laboratory studies have proved useful in making quite accurate predictions in geophysical and engineering problems (for example, see the discussion by Cushman-Roisin 1981).

Turbulent entrainment across a density interface in the presence of shear has an added complexity due to stratification and seems to differ greatly from the homogeneous mixing layer which has been studied extensively since Liepmann & Laufer (1948). Unlike the case of a homogeneous or weakly stratified shear layer, where the large scale coherent vortices and vortex pairing play a dominant role in the mixing process (Brown & Roshko 1974; Winant & Browand 1974; Koop & Browand 1979; Gartrell 1979), a high-Richardson-number, stratified mixing-layer is composed of events such as generation and breaking of waves, interchange of energy between waves and the mean flow and local shear-instabilities of the waves. In a certain sense, at high Richardson numbers, the density interface may act as a rigid boundary to the mixed-layer turbulence and it may be expected that the resulting wall-bounded shear flow will show some typical boundary-layer phenomena, such as boundary-layer streaks, vorticity amplification and bursting (Rao, Narasimha & Badri Narayanan 1971; Blackwelder & Eckelmann 1979). Indeed there is convincing evidence that such mechanisms enhance the entrainment in geophysical flows (Jackson 1976).

Due to the apparent direct applicability to oceanic and atmospheric situations, the shear-driven entrainment experiments of Kato & Phillips (1969), which are now considered classical, have drawn a great deal of attention from other researchers. These experiments were performed by applying, by a rotating screen, a constant shear stress on the surface of a linearly stratified fluid contained in an annulus. Their measurements indicated that the entrainment coefficient $E_* = u_e/u_*$, where u_e is the entrainment rate and u_* is the friction velocity, is a decreasing function of the bulk Richardson number $Ri_* = \Delta b h/u_*^2$ in which Δb is the buoyancy† jump across the interface and h is the average depth of the mixed layer. Similar experiments have been performed by Kantha, Phillips & Azad (1977) for two fluid systems, but entrainment rates were found to be about twice that of linearly stratified fluids for a given u_* and Ri_*. Based on the measurements of Linden (1975), Kantha *et al.* suggested that this may possibly be due to the energy losses associated with internal wave radiation from the base of the mixed layer into the linearly stratified region. However, Price (1979) and Thompson (1979) analysed the momentum budget for the annulus experiments and proposed that the sidewall frictional drag could introduce such differences in entrainment rates. Their analyses indicated that the entrainment law should be scaled with the mean velocity $\bar{u}$ of the mixed layer, rather than u_* and that the entrainment law in the presence of sidewall drag should take the form

$$E_v = \frac{u_e}{\bar{u}} = f(Ri_u),$$

with $Ri_u = \Delta b h/\bar{u}^2$.

Under these conditions, the suggested entrainment relation is $E_v \propto Ri_u^{-4}$, whereas, when the sidewall effects play a negligible role, the law was shown to be $E_* \propto Ri_u^{\frac{1}{2}} Ri_*^{-\frac{1}{2}}$, where $Ri_u \approx 0.6$. Deardorff & Willis (1982) performed a series of experiments to investigate the validity of these predictions and found that their data support the

† Buoyancy is defined as $b = g(\rho - \rho_0)/\rho_0$ where ρ is the density, ρ_0 is the reference density and g is the gravitational acceleration.

$Ri_*^{-\frac{1}{2}}$ law only if multiplied by $Ri_u^{-1.4}$. Further, these experiments did not support the assumption that Ri_u is a constant and indicated that, due to the viscous diffusion of momentum, the interfacial jump in the turbulent mean velocity could be much less than the mean velocity in the mixed layer. (The interfacial velocity jump was defined as the difference between the mean mixed-layer velocity and the mean velocity at the greatest distance to which the mixed-layer fluid propagates.)

In a detailed study of stress-driven entrainment experiments in annular geometries, Scranton & Lindberg (1983) found that such a geometry leads to secondary circulations in the radial direction, which results in a substantial interfacial tilt. Following up this study, Deardorff & Yoon (1984) investigated the causes for such secondary flows and found that the uneven angular momentum distribution across the annulus, due to solid-body rotation of the screen, was the major cause for the observed secondary circulation. The resulting Ekman layer near the screen causes the fluid to possess radial mean velocity toward the outer wall and this, in turn, results in higher entrainment rates at the outer-wall region than at the inner-wall region.

The present work was motivated by the belief that, although several possible velocity scales may exist, the velocity jump across the interface Δu was the most suitable velocity scale for the entrainment at a sheared density interface. While, in many instances, Δu has been used as the scaling velocity for entrainment experiments (Phillips 1977*b*; Price, Mooers & Van Leer 1978), our reasoning for such a selection is different. Due to enhanced mean shear, one would expect that turbulence is mainly produced at the sidewalls, rotating screen and at the density interface. However, measurements of wall-bounded flows suggest that a major portion of the turbulence produced at the walls dissipates near the wall itself and that the portion which diffuses outwards, which is also mainly responsible for the turbulence in the mixed layer, is only a small fraction of the total amount (Hinze 1975, p. 648). To some extent this idea is supported by the experiments of Jones & Mulhearn (1983), who found that the nature of the sidewalls, whether rough or smooth, does not affect the entrainment rates substantially. On the basis of the arguments presented above, it appears that a major portion of the energy for turbulent mixing at the density interface may result from the shear production at the entrainment zone itself and therefore the most significant velocity scale is Δu.

The present experiments were carried out in a closed-loop water channel by driving the mixed-layer over the heavy quiescent layer using a disk pump. Such an arrangement has the advantage of being free of a rigid rotating screen at the fluid surface, which has been shown to be the cause for secondary circulations. Also, the absence of endwalls, which cause undesirable recirculating flow, makes these experiments more refined than the previous surface shear-free experiments of Ellison & Turner (1959) and Chu & Baddour (1984). In this paper we report the results of our investigations on the nature of the entrainment zone, interfacial instabilities and entrainment mechanism, which have been the subject of very few previous studies (Wyatt 1978; Koop & Browand 1979).

2. Experimental procedure

The experimental procedure and the measurement techniques are discussed in detail in a companion paper by Narimousa, Long & Kitaigorodskii (1986). The salient features of the experiment are outlined below.

The apparatus is a scaled-up model of the version developed by Odell & Kovasznay

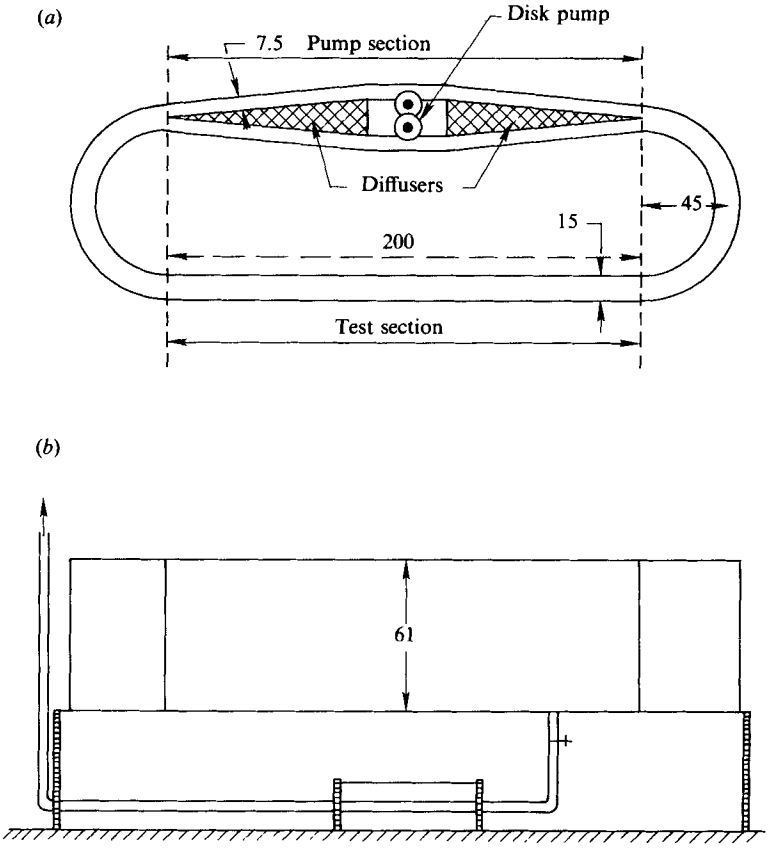

FIGURE 1. Schematic view of the experimental apparatus (all dimensions are in cm). (*a*) plan view (*b*) front view.

(1971) and is shown in figure 1. It is a closed loop water channel made of Plexiglas (1.25 cm thick). It has a straight test section 200 cm long. These two sections are joined by two semicircular annuli with a mean radius of 45 cm. Except at the pump section, the channel width is 15 cm; in order to have a constant cross-section throughout, two diffusers were placed in the pump section. These were of the same height as the channel (61 cm) and were placed in such a way as to create two narrower channels of width 7.5 cm. By placing a suitable number of disks only in the upper layer, the mixed-layer could be driven over the quiescent lower layer. The mean velocities in the upper layer were varied over the range 5–15 cm/s by changing the pump rotation rate. At the beginning of the experiments, the channel was stratified in two layers (fresh water and salt water). The experiment was started by turning on the disk pump.

Dye lines were released into the flow and the movement of the dye particles was filmed using a 16 mm camera. These films were later projected onto the pad of a digitizer and were analysed for the time-displacement characteristics of the dye particles by measuring the variation of their coordinates with time. Dye lines after 1 s of their release (or 0.5 s for high-mean-velocity experiments) were used to obtain the velocity profiles (figure 2) and hence the mean speed of the mixed-layer fluid, the thicknesses of the shear layer, and the viscous momentum diffusive layer. In the present experiments, the velocity attributed to the momentum diffusive layer was

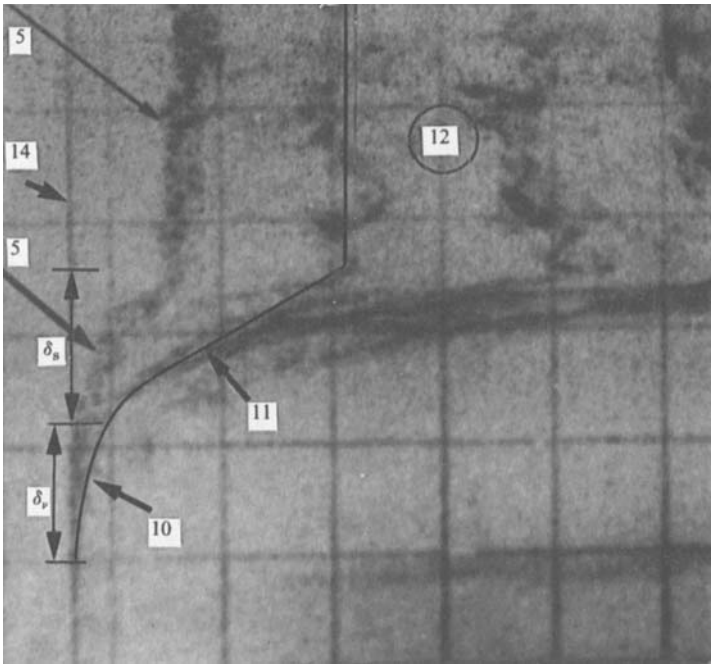

FIGURE 2. A representative velocity profile as indicated by a dye line. The positions of the shear layer (thickness δ_s) and the molecular diffusive layer (thickness δ_ν) are also indicated. *Key*: (1) entrainment interface; (2) the layered structure of the interfacial layer; (3) solitary waves in the interfacial layer; (4) large amplitude oscillations of the interfacial layer; (5) the subsequent appearance of the dye line; (6) region of intermediate density fluid located between the well mixed layer and the interfacial layer. This region can be identified by the irregular structure visible on a shadowgraph due to the partially mixed fluid parcels; (7) formation of regularly spaced billows at low Richardson numbers; (8) regions formed due to breakdown of billows. Note the existence of irregular small structure; (9) wave breaking at intermediate Richardson numbers. Note that wisps of fluid coming out of the wave crests; (10) momentum diffusive layer; (11) location of the shear layer; (12) upper homogeneous layer; (13) stable density interface; (14) location of the dye line (base line).

less than 15% of the mixed-layer mean velocity $\bar{u}$, while in some of the experiments of Deardorff & Willis (1982), it was reported to be nearly 40%. Hence, for scaling purposes, we have used the mean velocity of the mixed-layer as the velocity jump across the shear layer. To estimate the shear-layer thickness δ_s a straight line was fitted to the mid 50% of the velocity profile. This was done by selecting a large number of $u(z)$ *vs.* z data points in the regions $\frac{1}{4}\Delta u < u(z) < \frac{3}{4}\Delta u$ and fitting a line to these points. The distance (depth) between the intersection points of this line with the velocity profile corresponds to the mixed layer (in which the velocity is approximately constant) and the base line (figure 2) was considered as δ_s. This technique is similar to that used by Crapper & Linden (1974) to obtain density interfacial-layer thickness from conductivity profiles. The region between the exterior edge of the shear layer and the depth where $u(z) = 0$ can be considered to be the momentum diffusive layer.

The mixed-layer depth h was determined by recording the depth-density profiles using a single-electrode conductivity probe and an X–Y recorder. Since h was found to increase linearly with time, the entrainment rates $\mathrm{d}h/\mathrm{d}t$ could be easily calculated. The interfacial-layer wave heights were estimated using frame-by-frame analysis of

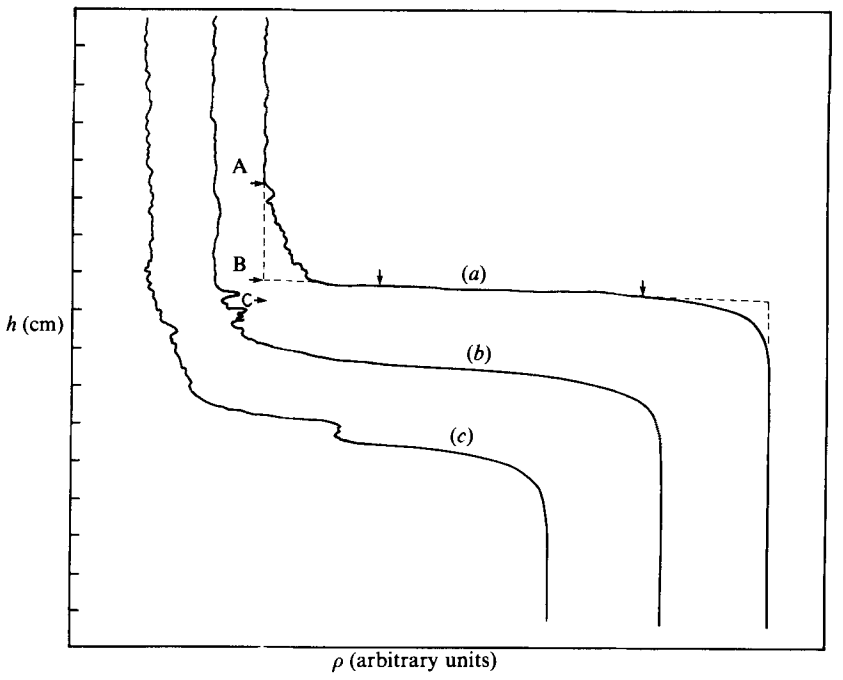

FIGURE 3. Three different types of density profiles observed during the entrainment process. Most of the profiles measured at high Ri_u were similar to the one shown in figure 3(*a*). However, occasionally profiles similar to those in figure 3(*b* and *c*) could be seen. AB = thickness of the intermediate layer; BC = thickness of the interfacial layer; the vertical arrows indicate the mid 50% of the interfacial layer profile.

the ciné films taken during the experiment as discussed in detail by Wyatt (1978). For a given h, about 10–15 waves were selected and analysed. Flow visualization was done using a thin sheet of laser light that scans the flow vertically to produce an image on a shadowgraph. The boundaries of the interfacial layer were quite distinct so that estimation of its thickness was possible. However, the presence of waves at the entrainment interface introduces uncertainties into these measurements. To overcome this problem, a large number of thickness measurements at a given h were made and averaged (Hopfinger & Toly 1976; Fernando & Long 1985*a*, *b*). The interfacial-layer thickness was also determined using the density profiles. Since the central region of the profile is linear, this was done by fitting a straight line to the mid 50% of the profile and by measuring the depth between the intersection points of this line and the density profiles corresponding to the well-mixed layer and the quiescent layer (figure 3*a*). The distance between the interior edge of the interfacial layer and the point of departure of the density profile from its value corresponding to the well-mixed layer can be considered as the intermediate-layer thickness. A straight-line fit to the profile in the intermediate zone can be used to obtain the buoyancy gradient within the layer. As shown in figure 3*b*, occasionally the intermediate density-zone contained 'wiggles'; in such cases the density gradients could not be determined.

During the course of an experiment, the mean velocity $\bar{u}$ decreases very slowly and hence the calculated Ri_u tends to increase. However, the measurements suggest that the variation of Ri_u above its initial value is less than 15%. Hence, in presenting the

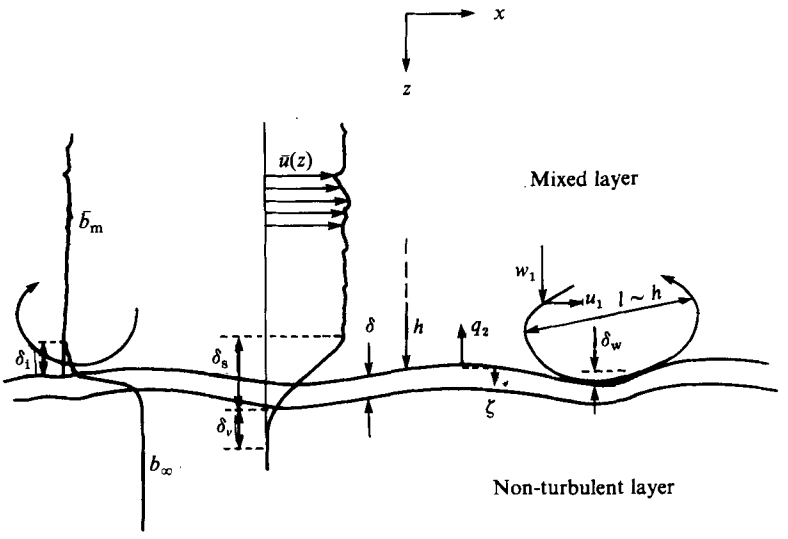

FIGURE 4. A simplified diagram of an entraining stratified fluid with interfacial shear drawn on the basis of the experimental observations. Note that the upper (h–δ_i) depth is well mixed. There is an intermediate layer (thickness δ_i) between the well-mixed layer and the interfacial layer with a weak but a measurable buoyancy gradient. The region encompassing the well-mixed layer and the intermediate layer is fully turbulent and is called the upper-mixed layer (thickness h). Shear layer (thickness δ_s) extends above the entrainment interface. Beneath it is the viscous momentum diffusive layer (thickness δ_v) that usually extends below the density interfacial layer. Also illustrated are the flattening of large eddies at the density interface and the scouring of the partially mixed fluid of the intermediate layer by the mixed layer eddies.

data we have used the mean value of the Richardson number for a given experiment. In evaluating the shear-layer thickness, the wave heights and the ratio of total buoyancy flux to the diffusive flux, the measurements were taken at different depths and averaged. In many of these cases the standard deviation (t-distribution) was less than 15% of the mean value. The uncertainties of measuring $\bar{u}$ and h were estimated to be 15% and 10%.

3. Principal experimental results

In this section we describe the qualitative observations and quantitative measurements made during the experiment. Possible theoretical explanations for the observed trends are given in §4.

3.1. *Qualitative observations*

Several interesting observations related to the entrainment process could be made during the experiments. At high Ri_u, a sharp, thin density-interfacial layer separated the turbulent and non-turbulent layers. The density in the well-mixed layer and the density gradient in the interfacial layer were found to be constant, but in some cases 'kinks' could be seen at the middle of the interfacial layer (figure 3*c*). According to Long (1973), this may be due to the existence of mixed regions within the stable layer, similar to those observed by Woods (1968) in the oceanic summer thermocline.The stability analysis of Phillips (1972) also demonstrates the possibility of the existence of 'kinks' in a sheared stable interface. At moderate and high Richardson numbers ($Ri_u > 5$), the density interfacial layer was found to be topped by a fluid

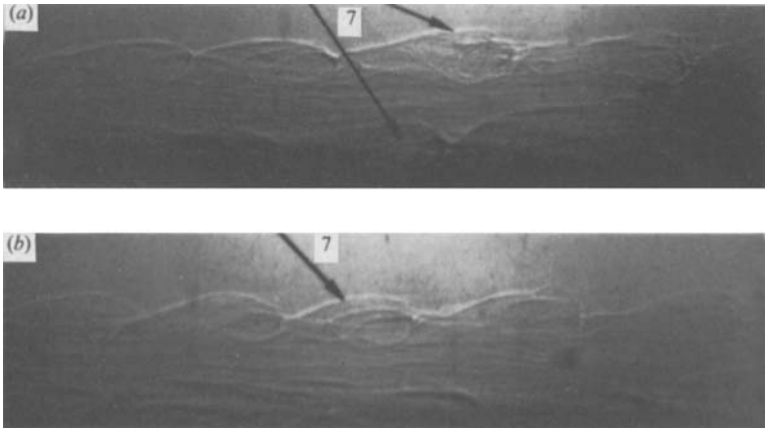

FIGURE 5. (*a*, *b*) Appearance of large coherent vortices at low Ri_u. See figure 2 for key.

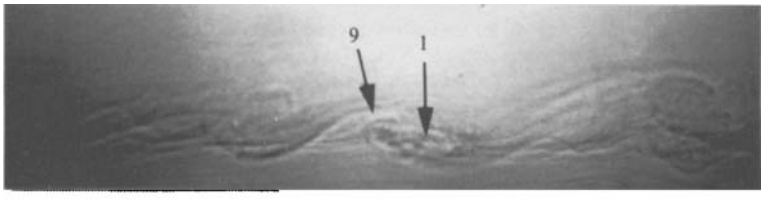

FIGURE 6. Breakdown of large vortices. See figure 2 for key.

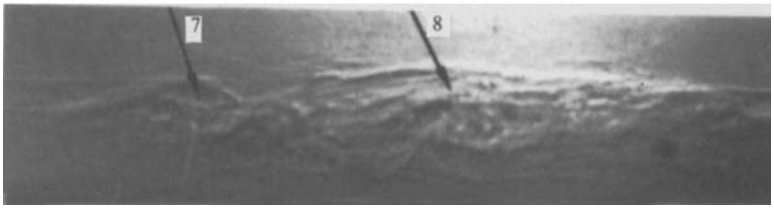

FIGURE 7. Appearance of breaking waves at high Ri_u. See figure 2 for key.

layer possessing a weak density gradient; it is conjectured that this layer consists of entrained fluid that has not yet been completely mixed. Above the intermediate layer, the fluid was quite homogeneous and no measurable density gradients could be detected. At low Richardson numbers where the entrainment rates are high, this layer appears to embrace the whole mixed-layer. The shear-layer velocity profile was observed to be linear in depth (figure 2) rather than logarithmic which one would expect if the mean-flow field was similar to the turbulent boundary layer over a flat plate. Below the shear layer, the velocity profile showed a resemblance to Couette flow which may be due to the viscous propagation of momentum as reported by Deardorff & Willis (1982). Based on these observations it is possible to deduce a *simplified* physical picture of the flow situation as shown in figure 4.

Observations on the nature of the interfacial instabilities showed that at low Richardson numbers ($Ri_u \lesssim 5$), the entrainment interface consists of regularly spaced billows (figure 5*a*, *b*) interconnected with thin braids within which the spatial variation of the density gradient is high. Such billow formation has been observed

FIGURE 8. Appearance of solitary waves at high Ri_u. See figure 2 for key.

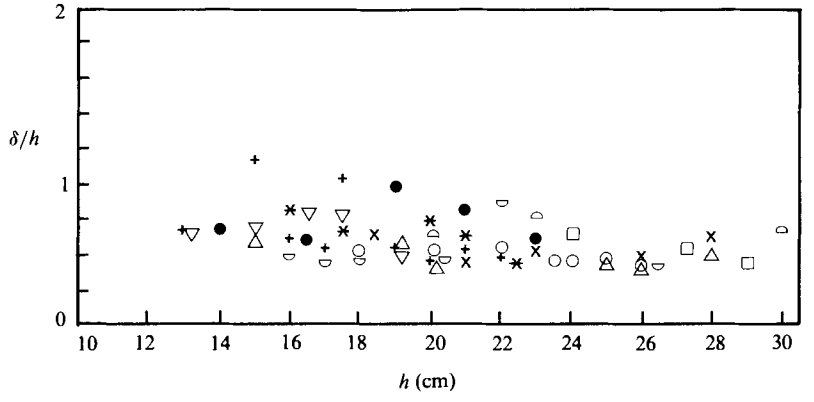

FIGURE 9. Variation of δ *vs.* h. The interfacial-layer thickness δ was evaluated using density profiles (e.g. figure 3).

in many previous low-Richardson-number, stratified mixing experiments (Thorpe 1971; Koop & Browand 1979; Gartrell 1979) and has been discussed by Corcos & Sherman (1976). The 'eye', or centre of the billows, consists of small-scale irregularities. According to Koop & Browand (1976), the generation of this fine structure may be due to the presence of local instability regions created during the entrainment of heavy and light fluid into the core region. However, their experiments indicate that the final stage of the mixing process (i.e. the homogenization by molecular diffusive effects) within the billows occurs slowly. Careful observations reveal that these billows ultimately break down to form regions containing an irregular small-scale structure (figure 6). Winant & Browand (1974) have proposed that mixed regions can also be formed by the interaction of two adjacent vortices. In some instances we were able to observe such interactions. As the Richardson number increased, the frequency of appearance of such billows decreased and the mixing seemed to be caused by a wave breaking process in which wisps of fluid are ejected to the mixed layer (figure 7). Such wave breaking events could be seen over a wide range of Richardson numbers ($5 \lesssim Ri_u \lesssim 20$) with a decrease in their occurrence with increasing Ri_u. Another interesting observation made at moderate Ri_u ($Ri_u \approx 10$–20) is the occurrence of large-amplitude solitary waves in the density interfacial layer; they travel through the layer and decay without breaking (figure 8). At Richardson number $Ri_u \gtrsim 20$, molecular processes seem to take over the entrainment mechanism as discussed in detail by Phillips (1977*b*) and by Narimousa *et al.* (1986).

3.2. *Thickness of the density interfacial layer*

The thickness δ of the density interfacial layer was determined by analysing the measured density profiles and the films containing shadowgraph observations.

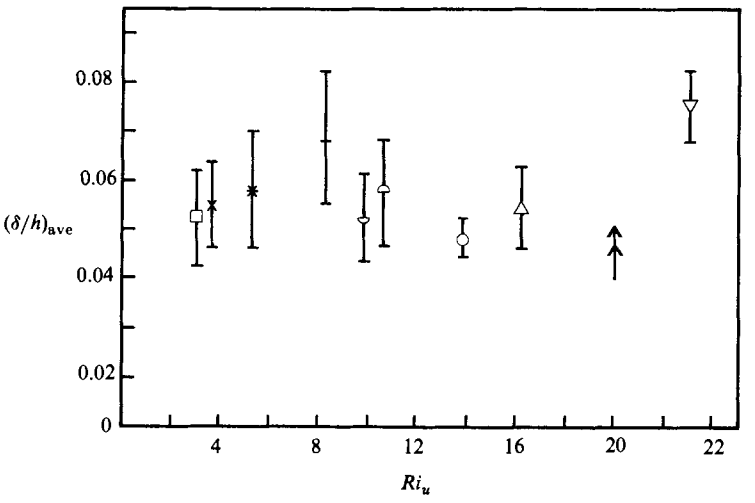

FIGURE 10. Variation of average (δ/h) *vs.* Ri_u for the experiments shown in figure 9. The arrow indicates the observed value of Ri_u at which the molecular diffusive effects take over the entrainment process. The error bars denote twice the standard deviation.

Figure 9 depicts the variation of δ with the mixed-layer depth as determined by the density profiles and indicates that $\delta \approx (0.04\text{–}0.08)\,h$. The scatter of the data may possibly be due to the oscillations of the interfacial layer as suggested by Fernando & Long (1985*a*). As evident from figure 10, the average δ/h (averaged over various h, for a given Ri_u) seems to be independent of Ri_u.

The variation of δ with h, evaluated using the shadowgraph observations are shown in figure 11. The solid line corresponds to $\delta \approx 0.07h$ and the results are consistent with the measurements made using the density profiles.

3.3. *Thickness of the shear layer*

The shear layer plays an important role in the entrainment process. Inasmuch as it is responsible for the production of turbulent kinetic-energy for mixing, it controls the size of the energy-containing eddies near the interface. Velocity profiles shown in figures 2 and 4 indicate the position and the nature of the shear layer. It appears that the shear layer (of thickness δ_s) penetrates into the highly stable density-interfacial layer while the mean velocity tends to zero within another layer (of size δ_v).

Figure 12 shows the variation of the non-dimensional shear-layer thickness δ_s/h with Ri_u. The results indicate that there is no significant variation of δ_s/h with Ri_u ($\delta_s \approx 0.20h$), suggesting that the energy-containing eddies at the entrainment zone should be scaled with h. By measuring the wave amplitude δ_w at the interfacial layer, Wyatt (1978) deduced that the shear-layer thickness should be independent of the mixed-layer depth. Wyatt's inference was based on numerical solutions of the Taylor–Goldstein equation by Hazel (1972) for a stratified shear layer which indicated that $\delta_w/\delta_s \approx$ constant and the observation that, in the experiments of Kantha *et al.* (1977), δ_w is independent of h for large Ri_u. The present study does not seem to support the above result. The application of Hazel's calculation to the present case may be doubtful in view of the marked differences in velocity and density profiles used in the calculations and observed in experiments and due to the presence of turbulence in the mixed layer which was not accounted for in Hazel's model.

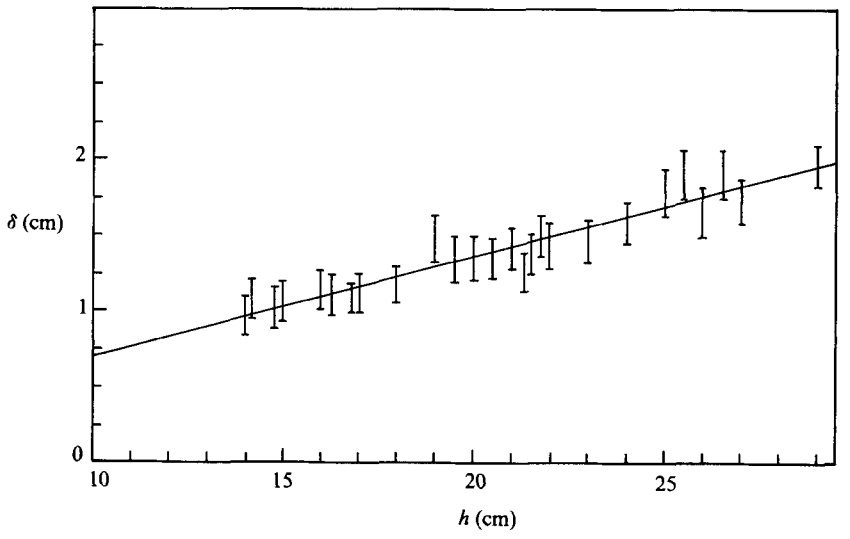

FIGURE 11. Variation of δ *vs.* h. In this case, δ was determined using the shadowgraph images. Maximum and minimum estimated values of δ at a given mixed-layer depth are indicated by the error bars.

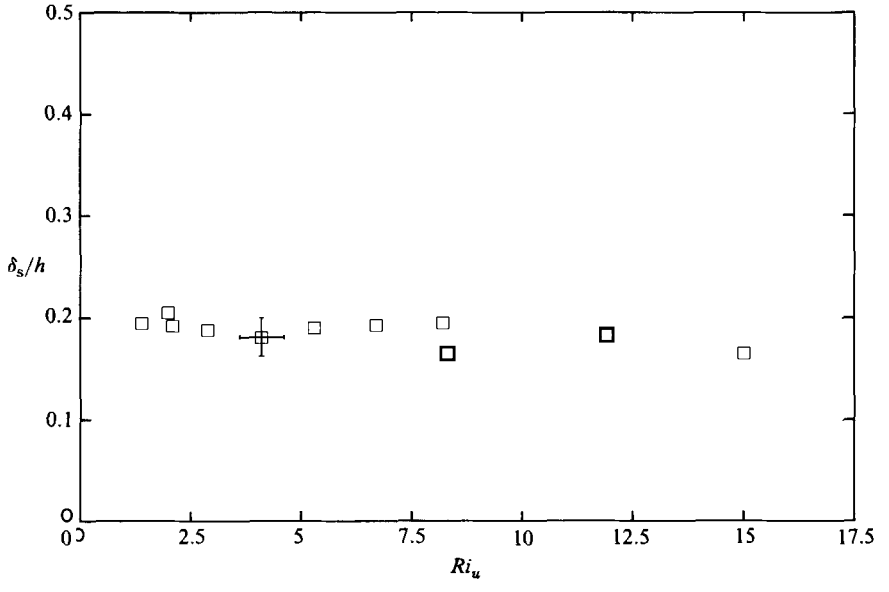

FIGURE 12. Variation of the non-dimensional shear layer thickness δ_s/h with the Richardson number.

According to Long (1973), the shear-layer thickness in the experiments of Moore & Long (1971) was found to decrease with Richardson number as $\delta_s/h \sim Ri_u^{-\frac{1}{2}}$ and this result also differs from those reported herein.

3.4. *Buoyancy flux at the entrainment zone*

As will be discussed in §4.1, the buoyancy flux at the entrainment interface can be calculated using $q_2 = -h\mathrm{d}\Delta b/\mathrm{d}t$. By using third-order spline fitting the data (Δb *vs.* t),

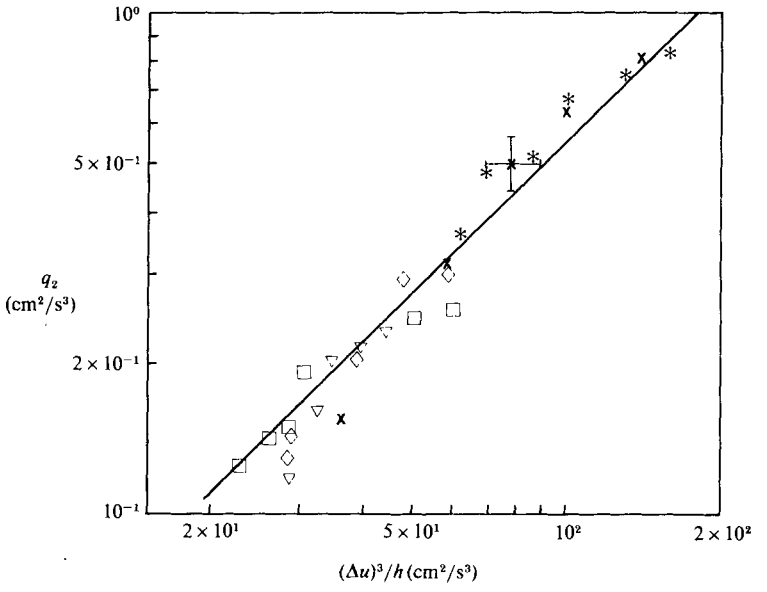

FIGURE 13. A log–log plot of estimated buoyancy flux (q_2) and $(\Delta u)^3/h$ for different Richardson numbers. ——, +1 slope.

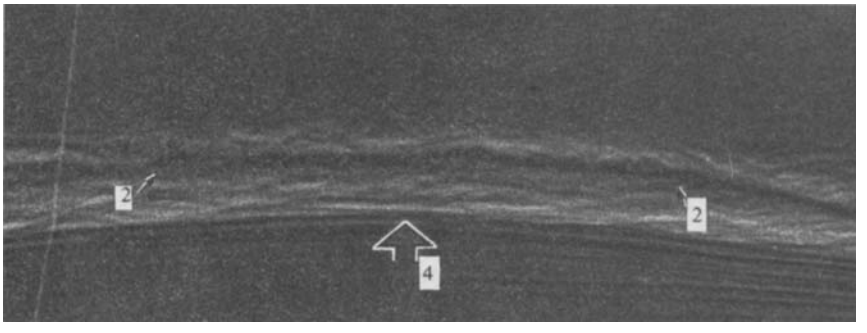

FIGURE 14. Oscillations of the interfacial layer. See figure 2 for key.

q_2 was calculated. A plot of q_2 *vs.* $(\Delta u)^3/h$ is shown in figure 13. It appears that q_2 is proportional to $(\Delta u)^3/h$, irrespective of Ri_u. The variable $(\Delta u)^3/h$ was selected in lieu of its proportionality to the rate of turbulent-energy production and dissipation in the mixing zone (§4.2).

3.5. *Interfacial waves*

The entrainment zone was complex in appearance and activities in this region depend on the Richardson number (§3.1). Visual observations indicated that the interfacial layer, as a whole, oscillates vertically (figure 14). Figure 15 shows the variation of the non-dimensionalized measured wave amplitudes δ_w/h with Ri_u. The solid line corresponds to the theoretical $Ri_u^{-\frac{1}{2}}$ behaviour obtained assuming that the waves are excited by the impingement of large eddies on the density interface (§4.4).

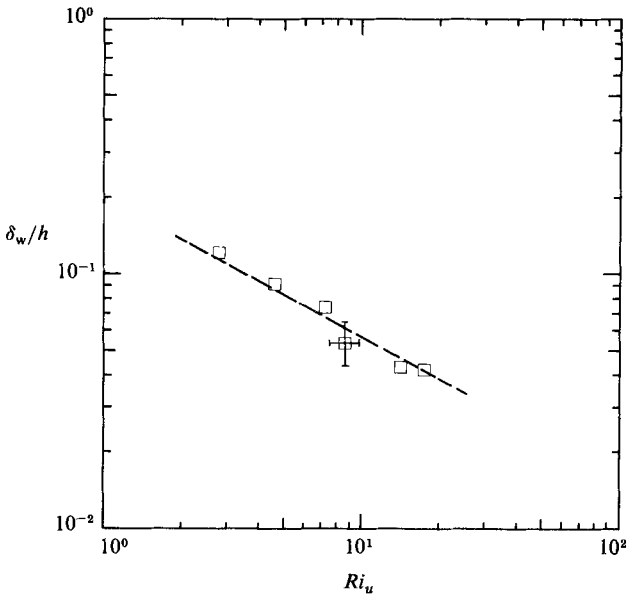

FIGURE 15. A log–log plot of δ_w/h *vs.* Ri_u. — —, 0.5 slope.

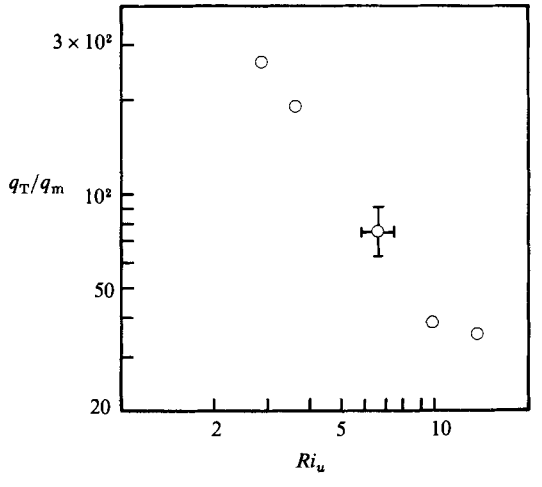

FIGURE 16. The variation of the ratio q_T/q_m with Ri_u.

3.6. *Molecular buoyancy transfer across the density interface*

The buoyancy flux across the entrainment interface consists of the turbulent flux and the molecular diffusive flux. Previous studies indicate that the relative contribution to the total flux from each of these is dependent on the Péclet number *Pe* (Crapper & Linden 1974; Piat & Hopfinger 1981) and the Richardson number (Phillips 1977*b*). At low Péclet numbers, or at very high Richardson numbers, the contribution of the molecular flux component can become dominant and molecular diffusive effects can take over the entire entrainment process. For the present experiments the molecular buoyancy flux q_d was calculated by measuring the buoyancy gradients in the interfacial layer and using $q_d = K_s \Delta b/\delta$, where K_s is the molecular diffusivity. The

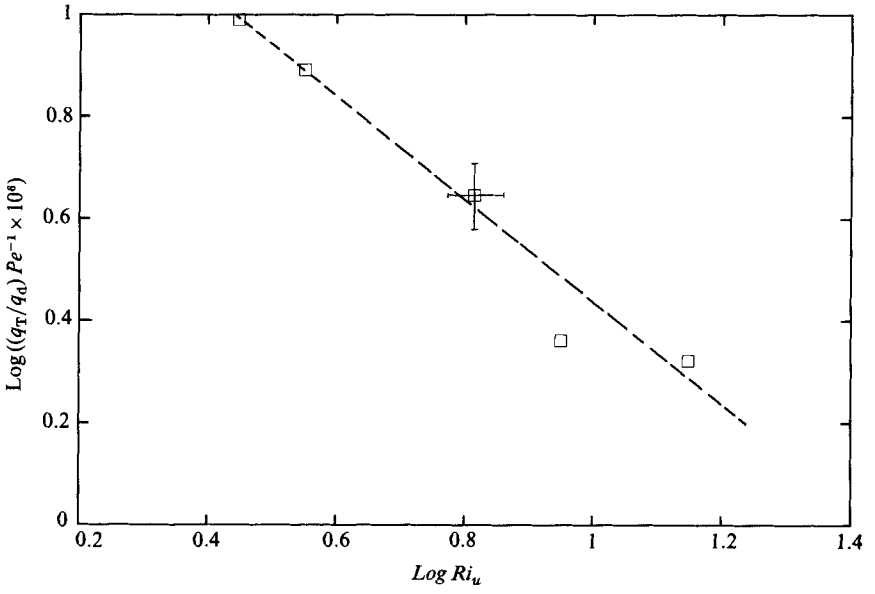

FIGURE 17. Variation of $\log((q_T/q_d)\,Pe^{-1} \times 10^6)$ with $\log Ri_u$ for five different experiments. – – –, -1 slope.

results are shown in figure 16 as a plot of q_T/q_d *vs.* Ri_u, where q_T is the entrainment flux due to turbulence alone. Note that for a wide range of Ri_u the molecular diffusive flux is only a small fraction of the total flux. Using the observations $q_T = -\overline{bw} \sim (\Delta u)^3/h$, $q_d = K_s \Delta b/\delta$ and $\delta \sim h$, it is possible to write $q_T/q_d \sim PeRi_u^{-1}$, which gives the proper normalizing variable for q_T/q_d. Figure 17 shows the variation of q_T/q_d *vs.* $PeRi_u^{-1}$ and lends support for the scaling arguments presented above.

The Péclet number $Pe = \Delta u h/K_s$ for our experiments was in the range 5×10^6–5×10^7. Although it is quite natural to expect large q_T/q_d values at such high Pe, the experiments of Piat & Hopfinger (1981) suggest that the molecular diffusion becomes predominant when $Pe < 2 \times 10^4$. To this end, the work of Crapper & Linden (1974) is also worthy of mention. They used shear-free turbulence induced by an oscillating grid to study the entrainment of heat- and salt-stratified fluids. In the salt-stratified experiments the interfacial layer contained wave activities including breaking, whereas in the heat-stratified experiments, a purely molecular 'diffusive core' instead of a turbulently-agitated interfacial layer was observed. According to Pearson & Linden (1983), the decay timescale for the internal waves is of the order $Pr^{-\frac{1}{2}}N^{-1}$, where Pr is the Prandtl number of the fluid and N is the buoyancy frequency. Hence we may suppose that, in heat-stratified experiments ($Pr \approx 10$), the internal waves that are generated 'smear' off quickly whereas in salt stratified experiments ($Pr \approx 1000$) the excited waves have enough time to grow and break thus causing mixing. However, the shear-driven, heat-stratified mixing experiments do not support the existence of a purely diffusive core. Substantial internal-wave activity has been detected in the heat-stratified interfacial layer (Piat & Hopfinger 1981) but whether they contribute directly to the turbulent entrainment has not yet been established. A further discussion on the influence of molecular diffusive effects in turbulent mixing in stratified flows is given in Fernando (1986).

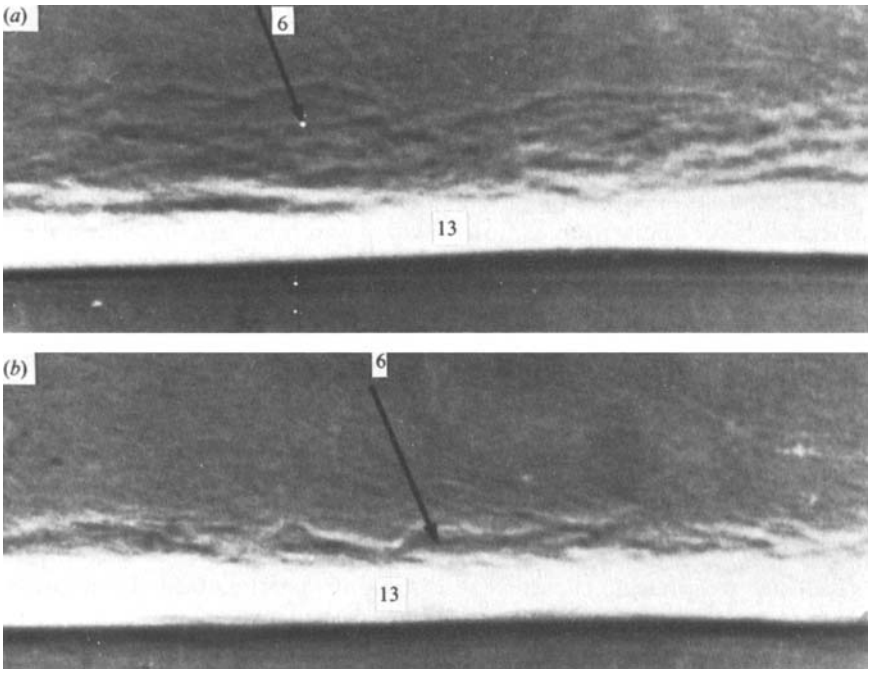

FIGURE 18. (*a*, *b*) Shadowgraph observations of the intermediate layer. See figure 2 for key.

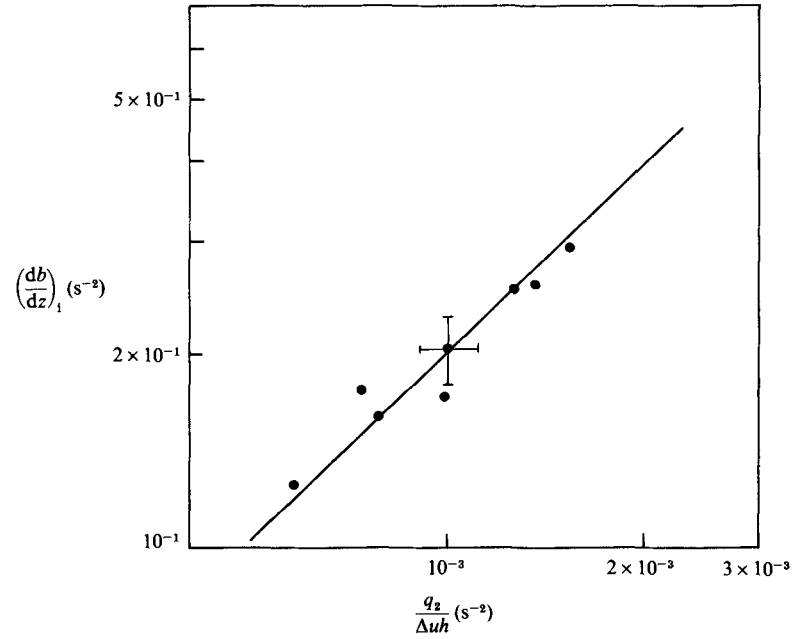

FIGURE 19. A log–log plot of $(db/dz)_i$ with $q_2/\Delta uh$. Here $(db/dz)_i$ is the density gradient of the intermediate density zone. ——, +1 slope.

3.7. *Development of an intermediate layer at the entrainment zone*

The formation of an intermediate layer between the well-mixed layer and the interfacial layer was discussed in §3.1 and is further illustrated in figure 18. Evidently, the intermediate layer contains partially mixed fluid resulting from the local mixing events that take place in the interior edge of the interfacial layer. At high Ri_u, the mixed-layer eddies are not energetic enough to engulf the fluid from the stable interfacial layer (Fernando & Long 1985*a*) and mixing can occur only by the breaking of waves that are excited by the mixed-layer turbulence. The locally mixed fluid thus forms a layer with a weak buoyancy gradient and the energy-containing eddies can entrain the fluid from this layer to the well-mixed layer.

Figure 19 depicts the variation of the buoyancy gradient in the intermediate layer $(\mathrm{d}b/\mathrm{d}z)_i$ with $q_2/\Delta uh$ for two of the experimental runs, and shows a linear correlation. The variables were selected in such a way as to test whether a simple gradient–transport model can be used to predict the buoyancy transfer across this layer.

4. Discussion of results

In this section, we present theoretical arguments pertinent to the experimental observations presented in §3.

4.1. *Conservation of buoyancy*

In view of the observation that the buoyancy in the mixed layer and the buoyancy gradient in the interfacial layer is constant, we may write

$$\bar{b} = b_\infty + \frac{\Delta b}{\delta}(z-h-\delta) \quad (h < z < h+\delta), \tag{1}$$

where $\bar{b}$ is the mean buoyancy, b_∞ is the density of the unperturbed layer and z is the vertical coordinate measured downwards from the free surface. Assuming horizontal homogeneity, one may integrate the buoyancy conservation equation

$$\frac{\partial \bar{b}}{\partial t} = \frac{\partial q}{\partial z} \quad \text{where } q = -\overline{bw}, \tag{2}$$

across the mixed layer and the interfacial layer (neglecting the intermediate zone of small density gradients) to yield (cf. Long 1978)

$$q(z) = q_2 \frac{z}{h} \quad (0 < z < h), \tag{3}$$

$$q_2 = -h\frac{\mathrm{d}(\Delta b)}{\mathrm{d}t}, \tag{4}$$

and

$$q(z) = q_2 + \frac{\mathrm{d}(\Delta b)}{\mathrm{d}t}\left\{\frac{\zeta^2}{2\delta} - \zeta\right\} - \frac{\mathrm{d}\delta}{\mathrm{d}t}\left[\frac{\Delta b \zeta^2}{2\delta^2}\right] - \frac{\Delta b}{\delta}\zeta\frac{\mathrm{d}h}{\mathrm{d}t} \quad (h < z < h+\delta), \tag{5}$$

where $q(z)$ is the buoyancy flux at any z, q_2 is the buoyancy flux at the entrainment interface and $\zeta = z-h$. Since $q(h+\delta) = 0$, one obtains

$$\frac{\mathrm{d}}{\mathrm{d}t}\Delta b(h+\tfrac{1}{2}\delta) = 0, \tag{6}$$

or

$$\Delta b(h+\tfrac{1}{2}\delta) = V_0^2, \tag{7}$$

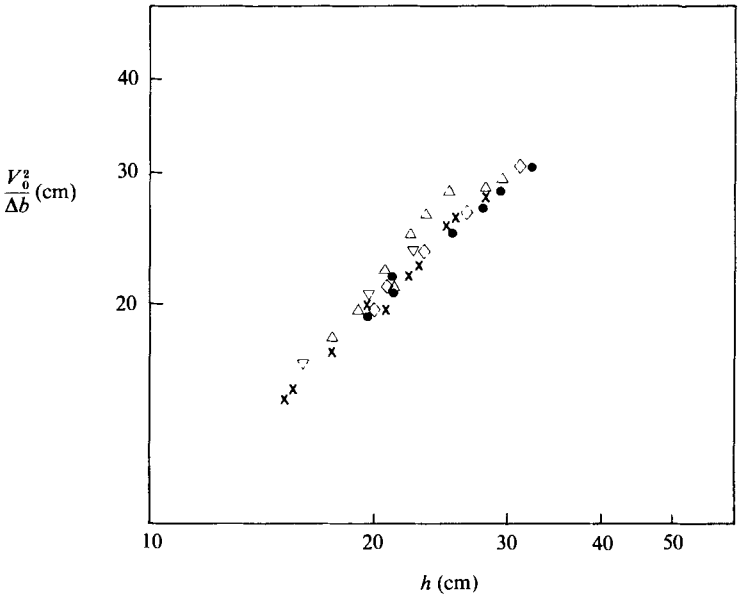

FIGURE 20. A log–log plot of $V_0^2/\Delta b$ *vs.* h for different experiments. ●, $Ri_u = 2.84$; ×, 3.55; ▽, 5.15; ◇, 5.80; △, 13.85.

where V_0 is the characteristic velocity scale based on the initial buoyancy jump and the depth of the upper homogeneous layer. Defining $V_0^2 = h_0 \Delta b_0$, where subscript '0' represents values at $t = 0$ (Fernando & Long 1983), and if $\delta = \alpha h$, (7) becomes

$$h(1 + \tfrac{1}{2}\alpha) = \frac{V_0^2}{\Delta b}. \tag{8}$$

A log–log plot of $V_0^2/\Delta b$ *vs.* h is shown in figure 20 and indicates that α can be considered as a constant with an average $\delta \approx 0.06h$. This result is consistent with the observations described in §3.2 and the results reported in Moore & Long (1971), Wolanski & Brush (1975) and Fernando & Long (1985*a*, *b*).

Note that $\delta = \alpha h$ where α is a constant, implies that $q_2 \sim u_e \Delta b$. In the mixed layer, where the turbulence is intense, we may write

$$-\overline{bw} \sim b_1 w_1 \sim u_e \Delta b, \tag{9}$$

where b_1, w_1 and u_1 are the r.m.s. values of the buoyancy, vertical and horizontal velocity fluctuations in the mixed layer. This, together with the fact that $u_1 \sim w_1 \sim \Delta u$ (Moore & Long 1971; Hunt 1983) give

$$\frac{b_1}{\Delta b} \sim \frac{u_e}{\Delta u} \sim Ri_u^{-n} \quad (n > 0), \tag{10}$$

where an entrainment law of the form $u_e/\Delta u \sim Ri_u^{-n}$ has been assumed.

It is also interesting to compare the kinetic (KE) and potential (PE) energies of the energy bearing eddies (of size h) in the mixed layer. We get

$$\frac{\text{KE}}{\text{PE}} = \frac{(\Delta u)^2}{b_1 h} \sim Ri_u^{n-1}. \tag{11}$$

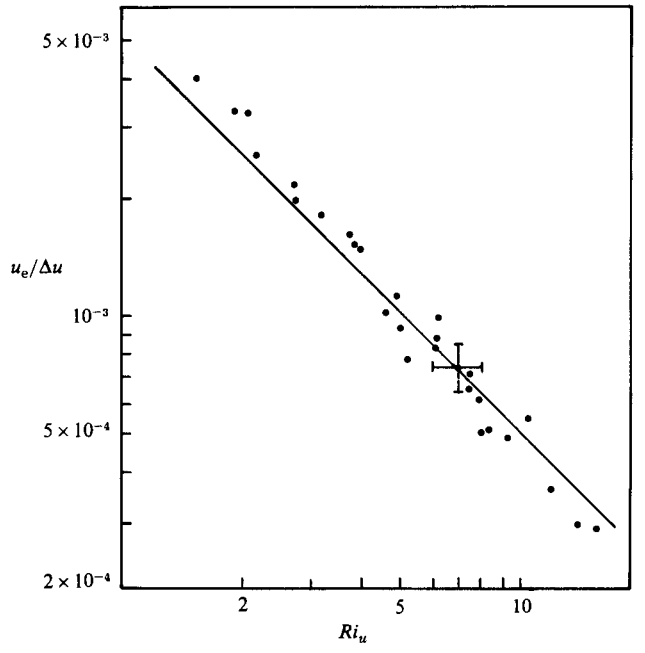

FIGURE 21. The entrainment law: A log–log plot of $u_e/\Delta u$ *vs.* Ri_u. ——, −1 slope.

If $n = 1$, as indicated by some experiments (§4.2), then KE/PE = $O(1)$ and hence kinetic and potential energies of the large-scale mixed-layer eddies are of the same order.

4.2. *Energy budget at the entrainment interface*

The energy equation for the interfacial region can be written as

$$-\overline{uw}\frac{d\bar{u}}{dz}+\overline{bw}-\epsilon \approx 0, \tag{12}$$

where the first and last terms represent the turbulent energy production and dissipation, and the flow is assumed to be quasi-stationary and horizontally homogeneous. The turbulent-energy diffusion in the vertical direction is assumed to be relatively small compared to the production. The latter assumption is based on the observation that, in the shear zone of a turbulent boundary layer, the principal contributions to the energy budget come from the production and dissipation terms (Ellison 1957). Measurements in both homogeneous and stratified turbulent flows suggest $-\overline{uw} \sim u_1^2$ (Hinze 1975, p. 643; Ellison 1962) and $u_1 \sim \Delta u$ (Moore & Long 1971) and hence the kinetic energy production can be parameterized by $-\overline{uw}\,d\bar{u}/dz \sim (\Delta u)^3/\delta_s \sim (\Delta u)^3/h$. We may also estimate the kinetic energy dissipation at the entrainment interface as $\epsilon \sim (\Delta u)^3/\delta_s \sim (\Delta u)^3/h$ (Townsend 1958), where is it assumed that below the scales of h, the buoyancy effects are unimportant (§4.1). This parameterization together with the observation that $\overline{bw}(-q_2) \sim (\Delta u)^3/h$ (figure 13) yield $q_2 \sim -\overline{uw}\,d\bar{u}/dz \sim \epsilon$. There are several interesting consequences of this result, namely: (i) at the entrainment interface the buoyancy flux, dissipation and the energy production are of the same order, and the flux Richardson number $R_f = (\overline{bw}/\overline{uw}\,d\bar{u}/dz)$ is a constant; (ii) since $-\overline{bw} \sim u_e \Delta b \sim \Delta u^3/h$, the basic entrainment law becomes $E \sim u_e/\Delta u \sim Ri_u^{-1}$, which is not inconsistent with the present observations

that indicate $E \sim Ri_u^{-n}$ behaviour with $n = 1.0$–1.2 (figure 21) and also with many other previous experiments; (iii) the mixed-layer depth is proportional to the Monin–Obukhov lengthscale, i.e. $h \sim -(\Delta u)^3/\overline{bw}$ (see also Long 1975); and (iv) the gradient Richardson number $Ri_G = \Delta b \delta_s^2/\delta(\Delta u)^2$ is proportional to Ri_u, which is in agreement with the observations of Kranenburg (1984).

The result $q_2/(\Delta u^3/h) \approx 5.5 \times 10^{-3}$ obtained from figure 13 can be used to estimate R_f. The production term in (12) can be estimated as $-\overline{uw}\,\mathrm{d}\bar{u}/\mathrm{d}z \approx c_1 u_1^2\,\mathrm{d}\bar{u}/\mathrm{d}z \approx c_1 u_1^2(\Delta u)/\delta_s$, where $c_1 \approx 0.25$ (Ellison 1962). Using $u_1 \approx 0.13(\Delta u)$ (Moore & Long 1971) and $\delta_s \approx 0.20h$, we get $-\overline{uw}\,\mathrm{d}\bar{u}/\mathrm{d}z \approx 2.11 \times 10^{-2}(\Delta u)^3/h$. Hence, $R_f = (\overline{bw}/\overline{uw})\,(\mathrm{d}\bar{u}/\mathrm{d}z) \approx 0.26$, which agrees well with the measurements of McEwan (1983) who found $R_f = 0.26 \pm 0.064$. Also using (12), we obtain $\epsilon \approx -0.74\overline{uw}\,\mathrm{d}\bar{u}/\mathrm{d}z \approx 1.56 \times 10^{-2}(\Delta u)^3/h$. Comparing the above expression with $\epsilon \approx u_1^3/l$ (Batchelor 1953), where l is the integral lengthscale of turbulence, gives $l \approx 0.14h$ which is consistent with the argument that the turbulent energy at the entrainment zone is mainly produced due to interfacial shear at the scales of the order δ_s ($\approx 0.20h$).

4.3. *Amplitude of the interfacial waves*

It is possible to explain the results presented in §3.4 by assuming that the wave undulations are due to the energy-containing, mixed-layer eddies impinging on the density interface. If the wave amplitudes are determined by a balance between the vertical kinetic energy of the eddies w_1^2 and the potential energy content of the generated waves approximately $N^2\delta_w^2$, we get

$$\delta_w \sim \frac{w_1}{N}, \tag{13}$$

where N is the boundary frequency of the interfacial layer. Since $N = (\Delta b/\delta)^{\frac{1}{2}}$, $\delta \sim h$, and $w_1 \sim (\Delta u)$, (13) can be written as

$$\frac{\delta_w}{h} \sim Ri_u^{-\frac{1}{2}}, \tag{14}$$

which agrees well with the experimental results presented in figure 15.

4.4. *Buoyancy transfer process across the entrainment interface*

The observation, $q_2 \sim \Delta u h(\mathrm{d}b/\mathrm{d}z)_i$, suggests that the buoyancy transfer process across the intermediate density zone can be described by a simple gradient-transport model in which the eddy viscosity is parametrized with the size (of the order of h) of the energy containing eddies and the r.m.s. velocity (of the order of Δu) near the interface. This observation is consistent with the notion that the intermediate density fluid is carried to the mixed layer by the energy containing eddies. It should be noted that although a simple gradient–transport model can predict the buoyancy transfer across the weakly stable intermediate layer, turbulence in strongly stratified fluids is confined to intermittently occurring turbulent patches and the buoyancy transfer process can be quite complicated.

5. Summary

(i) When a mean flow is generated over a density interface, the shear-generated turbulence causes mixing and turbulent entrainment across the density interface. Estimates show that, at the entrainment zone, the rates of work done against the

buoyancy forces, kinetic energy dissipation and shear-production of turbulent kinetic energy are of the same order so that the flux Richardson number is a constant.

(ii) During the entrainment process, two layers (namely, the density interfacial layer and the shear layer) that have a direct bearing on the entrainment process develop. The former is thinner than the latter but both tend to grow linearly with the mixed-layer depth independent of the Richardson number.

(iii) The mixing mechanism appears to be different for different Richardson number ranges. At low Richardson numbers the shear layer exhibited the formation and breakdown of large, ordered vortices whereas, at intermediate Richardson numbers, sporadic wave breaking seemed to be the major cause of mixing.

(iv) The density interfacial layer showed wave oscillations whose amplitudes scale well with the estimated size of the undulations caused by the impingement of large eddies of the size of the mixed layer, at the density interfacial layer.

(v) When the Péclet number is high, the molecular buoyancy flux across the entrainment interface is negligible compared to the turbulent flux, even at moderately high Richardson numbers.

(vi) Locally mixed fluid that has not yet been taken to the well-mixed layer forms a layer of mixed fluid of density intermediate to the well-mixed layer and the interfacial layer. This layer has a density gradient which is small compared to the density interfacial layer but large compared to that of the mixed layer. Evidently the fluid in this intermediate layer is transported to the well-mixed layer by energy-bearing eddies of the latter and the buoyancy transfer process across the intermediate layer can be described by a gradient–transport model.

We wish to thank Professors Phillips, Long, Kitaigorodskii, and Corrsin for their invaluable support during the initial phase of this work. Also thanks are due to Professor E. John List for his kind cooperation, Professors T. Maxworthy, D. F. Jankowski, P. Neitzel, and G. Oth for their friendship. This work was supported by NSF grant nos. CEE 7272A1 and MSM 8504909 and ONR Contract no. N 0014-76-C-0184.

REFERENCES

BATCHELOR, G. K. 1953 *Theory of Homogeneous Turbulence.* Cambridge University Press.

BLACKWELDER, R. F. & ECKELMANN, H. 1979 Streamwise vortices associated with the bursting phenomena. *J. Fluid Mech.* **94**, 577.

BROWN, G. L. & ROSHKO, A. 1974 On density effects and a large structure in turbulent mixing layers. *J. Fluid Mech.* **64**, 775.

CHU, V. H. & BADDOUR, R. E. 1984 Turbulent gravity – stratified shear flows. *J. Fluid Mech.* **138**, 353.

CORCOS, G. M. & SHERMAN, F. S. 1976 Vorticity concentration and the dynamics of unstable free shear layers. *J. Fluid Mech.* **73**, 241.

CRAPPER, P. F. & LINDEN, P. F. 1974 The structure of the turbulent density interfaces. *J. Fluid Mech.* **65**, 45.

CUSHMAN-ROISIN, B. 1981 Deepening of the wind-mixed layer: a model of the vertical structure. *Tellus* **33**, 564.

DEARDORFF, J. W. & WILLIS, G. E. 1982 Dependence of mixed-layer entrainment on shear stress and velocity jump. *J. Fluid Mech.* **115**, 123.

DEARDORFF, J. W. & YOON, S. C. 1984 On the use of an annulus to study mixed-layer entrainment. *J. Fluid Mech.* **142**, 97.

ELLISON, T. H. 1957 Turbulent transport of heat and momentum from an infinitely rough plane. *J. Fluid Mech.* **2**, 456.

ELLISON, T. H. 1962 Laboratory measurements of turbulent diffusion in stratified flows. *J. Geophys. Res.* **67**, 3029.

ELLISON, T. H. & TURNER, J. S. 1959 Turbulent entrainment in stratified flows. *J. Fluid Mech.* **6**, 423.

FERNANDO, H. J. S. 1986 Molecular diffusive effects in stratified turbulent mixing. *Advancements in Aerodynamics, Fluid Mechanics, and Hydraulics* (eds. R. E. A. Arndt, H. G. Stefan, C. Farell & S. M. Peterson).

FERNANDO, H. J. S. & LONG, R. R. 1983 The growth of a grid generated turbulent mixed-layer in a two fluid system. *J. Fluid Mech.* **133**, 377.

FERNANDO, H. J. S. & LONG, R. R. 1985*a* On the nature of the entrainment interface of a two-layer fluid subjected to zero-mean-shear turbulence. *J. Fluid Mech.* **151**, 21.

FERNANDO, H. J. S. & LONG, R. R. 1985*b* The growth of a shear free mixed layer in a linear stratified fluids. *Phys. Fluids* **28**, 2999.

FISCHER, H., LIST, J., KOH, R., IMBERGER, J. & BROOKS, N. 1979 *Mixing in Inland and Coastal Waters.* Academic.

GARTRELL, G. 1979 Studies on the mixing in a density stratified shear flow. Ph.D. thesis, California Institute of Technology (W. M. Keck Laboratory, Report No. KH-R-39).

HAZEL, P. 1972 Numerical studies of the stability of inviscid stratified shear flows. *J. Fluid Mech.* **51**, 39.

HOPFINGER, E. J. & TOLY, J.-A. 1976 Spatially decaying turbulence and its relation to mixing across density interfaces. *J. Fluid Mech.* **78**, 155.

HINZE, J. O. 1975 *Turbulence.* McGraw-Hill.

HUNT, J. C. R. 1983 Turbulence structure and turbulent diffusion near gas–liquid interface. In *Proc. Intl Symp. Gas Transfer across Water Surfaces, Ithaca, NY* (ed. W. Brutsaert & G. H. Jirka).

JACKSON, R. G. 1976 Sedimentological and fluid dynamic implication of the turbulent bursting phenomena in geophysical flows. *J. Fluid Mech.* **77**, 531.

JONES, I. S. F. & MULHEARN, P. J. 1983 The influence of external turbulence on sheared interfaces. *Geophys. Astrophys. Fluid Dyn.* **24**, 49.

KANTHA, L. H., PHILLIPS, O. M. & AZAD, R. S. 1977 On turbulent entrainment at a stable density interface. *J. Fluid Mech.* **79**, 753.

KATO, H. & PHILLIPS, O. M. 1969 On the penetration of a turbulent layer into stratified fluid. *J. Fluid Mech.* **37**, 643.

KOOP, C. G. & BROWAND, F. K. 1979 Instability and turbulence in a stratified fluid with shear. *J. Fluid Mech.* **93**, 135.

KRANENBURG, C. 1984 Wind-induced entrainment in a stably stratified fluid. *J. Fluid Mech.* **145**, 253.

LIEPMANN, H. W. & LAUFER, J. 1948 Investigations of free turbulent mixing. *NACA (Wash.) Tech. Note* no. 1257.

LINDEN, P. F. 1975 The deepening of a mixed-layer in a stratified fluid. *J. Fluid Mech.* **71**, 385.

LONG, R. R. 1973 Some properties of horizontally homogeneous, statistically steady turbulence in a stratified fluid. *Boundary-Layer Met.* **5**, 139.

LONG, R. R. 1975 The influence of shear on mixing across density interfaces. *J. Fluid Mech.* **70**, 305.

LONG, R. R. 1978 A theory of mixing in a stably stratified fluid. *J. Fluid Mech.* **84**, 113.

MCEWAN, A. D. 1983 Internal mixing in stratified fluids. *J. Fluid Mech.* **128**, 59.

MOORE, M. J. & LONG, R. R. 1971 An experimental investigation of turbulent stratified shearing flow. *J. Fluid Mech.* **49**, 635.

NARIMOUSA, S., LONG, R. R. & KITAIGORODSKII, S. A. 1986 Entrainment due to turbulent shear flow at the interface of a stably stratified fluid. *Tellus* **38A**, 76.

ODELL, G. M. & KOVASZNAY, L. S. G. 1971 A new type of water channel with density stratification. *J. Fluid Mech.* **50**, 535.

PEARSON, H. J. & LINDEN, P. F. 1983 The final stage of decay of turbulence in stably stratified fluid. *J. Fluid Mech.* **134**, 195.

PHILLIPS, O. M. 1972 Turbulence in a strongly stratified fluid. – Is it Unstable? *Deep-Sea Res.* **19**, 79.

PHILLIPS, O. M. 1977*a* *Entrainment, Modelling and Prediction of the Upper Layers of the Ocean* (ed. E. G. Kraus). Pergamon.

PHILLIPS, O. M. 1977*b* *Dynamics of the Upper Ocean.* Cambridge University Press.

PIAT, J. F. & HOPFINGER, E. J. 1981 A boundary layer topped by a density interface. *J. Fluid Mech.* **113**, 411.

PRICE, J. F. 1979 On the scaling of stress-driven entrainment experiments. *J. Fluid Mech.* **90**, 509.

PRICE, J. F., MOOERS, C. N. K. & VAN LEER, J. C. 1978 Observation and simulation of storm-induced mixed-layer deepening. *J. Phys. Oceanogr.* **8**, 582.

RAO, K. N., NARASIMHA, R. & BADRI NARAYANAN, M. A. 1971 The bursting phenomenon in a turbulent boundary layer. *J. Fluid Mech.* **48**, 339.

SCRANTON, D. R. & LINDBERG, W. R. 1983 An experimental study of entraining stress-driven, stratified flow in an annulus. *Phys. Fluids* **26** (5), 1198.

THOMPSON, R. O. R. Y. 1979 A re-examination of entrainment process in some laboratory flows. *Dyn. Atmos. Oceans* **4**, 45.

THORPE, S. A. 1971 Experiments of the instability of stratified shear flows: miscible fluids. *J. Fluid Mech.* **46**, 299.

TOWNSEND, A. A. 1958 Turbulent flows in stably stratified atmosphere. *J. Fluid Mech.* **3**, 361.

WINANT, C. D. & BROWAND, F. K. 1974 Vortex pairing: The mechanism of turbulent mixing layer growth at moderate Reynolds number. *J. Fluid Mech.* **63**, 237.

WOLANSKI, E. J. & BRUSH, L. M. 1975 Turbulent entrainment across stable density step structures. *Tellus*, **27**, 259.

WOODS, J. D. 1968 Wave induced shear instability in the summer thermocline. *J. Fluid Mech.* **32**, 791.

WYATT, L. R. 1978 The entrainment interface in a stratified fluid. *J. Fluid Mech.* **86**, 293.